Eur. Phys. J. B **47**, 213–220 (2005)
DOI: 10.1140/epjb/e2005-00320-3

THE EUROPEAN PHYSICAL JOURNAL B

Structural anomalies associated with the electronic and spin transitions in $LnCoO_3$

K. Knížek[1,a], Z. Jirák[1], J. Hejtmánek[1], M. Veverka[1], M. Maryško[1], G. Maris[2], and T.T.M. Palstra[2]

[1] Institute of Physics ASCR, Cukrovarnická 10, 162 53 Prague 6, Czech Republic
[2] Solid State Chemistry Laboratory, Materials Science Centre, University of Groningen, Nijenborg 4, 9747 AG Groningen, The Netherlands

Received 4 March 2005 / Received in final form 12 June 2005
Published online 11 October 2005 –

Abstract. A powder X-ray diffraction study, combined with magnetic susceptibility and electric transport measurements, was performed on a series of $LnCoO_3$ perovskites (Ln = Y, Dy, Gd, Sm, Nd, Pr and La) over a temperature range 100–1000 K. A non-standard temperature dependence of the observed thermal expansion was modelled as a sum of three contributions: (1) weighted sum of lattice expansions of the cobaltite in the diamagnetic low spin state and in the intermediate (IS) or high (HS) spin state. (2) An anomalous expansion due to the increasing population of excited (IS or HS) states of Co^{3+} ions over the course of the diamagnetic-paramagnetic transition. (3) An anomalous expansion due to excitations of Co^{3+} ions to another paramagnetic state accompanied by an insulator-metal transition. The anomalous expansion is governed by parameters that are found to vary linearly with the Ln ionic radius. In the case of the first magnetic transition it is the energy splitting E between the ground low spin state and the excited state, presumably the intermediate spin state. The energy splitting E, determined by a fit to magnetic susceptibility, decreases with temperature. The values of E determined for $LaCoO_3$ and $YCoO_3$ at $T = 0$ K are 164 K and 2875 K respectively, which fall to zero at $T = 230$ K for $LaCoO_3$ and 860 K for $YCoO_3$. The second anomalous expansion connected with a simultaneous magnetic and insulator-metal transition is characterized by its center at $T = 535$ K for $LaCoO_3$ and 800 K for $YCoO_3$. The change of the unit cell volume during each transition is independent of the Ln cation and is about 1% in both cases.

PACS. 61.10.Nz X-ray diffraction – 71.30.+h Metal-insulator transitions and other electronic transitions

1 Introduction

The magnetic and electric transport properties of rare-earth cobalt perovskites $LnCoO_3$ (Ln = La, Y, rare-earth) have had most detailed study on $LaCoO_3$. At low temperatures $LaCoO_3$ is nonmagnetic, Co^{3+} ion being in the LS state with six electrons in the t_{2g} levels and empty e_g states (LS, $t_{2g}^6 e_g^0$, $S = 0$). At 50–100 K $LaCoO_3$ undergoes a transition to a magnetic state, the character of which is still under intense debate. Its origin is in a thermal population of excited Co^{3+} states that are either of intermediate spin (IS, $t_{2g}^5 e_g^1$, $S = 1$) or high spin (HS, $t_{2g}^4 e_g^2$, $S = 2$) character. A second transition at 500–550 K is of an insulator-metal (I-M) kind and is accompanied by a further change of paramagnetic properties.

The analogous compound $YCoO_3$ also undergoes a diamagnetic-paramagnetic transition, but more diffusive and shifted to higher temperatures between 450 and 800 K [1]. The I-M transition occurs around 750 K.

The temperatures of the magnetic transitions of the other $LnCoO_3$ perovskites are difficult to determine by magnetic susceptibility measurement due to the large magnetic moment of the rare-earth element, which masks a possible change of the magnetic state of cobalt. However, recently Yan et al. [2] determined the magnetic transitions of $PrCoO_3$ and $NdCoO_3$ by subtracting a magnetic susceptibility of the corresponding $LnAlO_3$. They determined that the excitation to IS or HS states begins at 35 K, 200 K and 300 K for $LaCoO_3$, $PrCoO_3$ and $NdCoO_3$, respectively. Information on the spin state transition has also been deduced using temperature dependent infrared spectroscopy [3]. The spectra of $LnCoO_3$ single-crystals revealed anomalies in $LaCoO_3$, $PrCoO_3$ and $NdCoO_3$ around 120, 220 and 275 K, respectively. At these temperatures a decrease of the intensities of stretching and bending modes associated with the LS state was observed, which was accompanied by an increase of new bands ascribed to the IS state.

As to the I-M transitions in the $LnCoO_3$ series, the published resistivity data show a clear correlation with the

[a] e-mail: knizek@fzu.cz

ionic radius of Ln cations. The transition temperature, defined as the maximum in activation energy of electrical resistivity, thus increases systematically and is shifted from 500 K for $LaCoO_3$ to 650 K for $GdCoO_3$ [4] and 750 K for $YCoO_3$ [1].

The magnetic and electronic transitions are accompanied also by subtle changes in the crystal structure, which is of the rhombohedral perovskite type $R\bar{3}c$ for $LaCoO_3$ and the orthorhombic $Pbnm$ type for the other $LnCoO_3$ with smaller rare-earth or yttrium cations. The effects are of two kinds. First, the ionic radius of Co^{3+} increases from $r_{LS} = 0.545$ Å to $r_{IS} = 0.56$ Å or $r_{HS} = 0.61$ Å [5]. Second, Co^{3+} ion in IS or HS state is Jahn-Teller active and corresponding distortion of the CoO_6 octahedra may arise. In particular, a monoclinic distortion of the $LaCoO_3$ structure (space group $I2/a$) and Jahn-Teller distortion of CoO_6 octahedra was found recently by single-crystal X-ray diffraction between 100 and 300 K [6].

The Co^{3+} size effect is responsible for an anomalous thermal expansion that reflects the increasing population of magnetic species. This was indeed observed for $LaCoO_3$ on single-crystal material around 50 K by dilatometry [7] and neutron scattering [8] and by powder neutron diffraction both around 50 K and second magnetic transition at 500–550 K [5,9]. High temperature X-ray diffraction revealed anomalous thermal expansion also for other $LnCoO_3$, namely Ln = Nd, Gd, Dy and Ho [10] and $YCoO_3$ and $LuCoO_3$ [11]. The characteristic temperatures of the structural anomalies shift to higher temperature with decreasing Ln ionic radius. Simultaneously, the onset of magnetic transition is shifted to ≈440 K for $YCoO_3$ and to ≈540 K for $LuCoO_3$ [11].

This paper reports on a structural and electric transport investigation of the $LnCoO_3$ series over a wide temperature range 100–1000 K. Our aim was to resolve different contributions to the thermal expansion in order to establish a quantitative basis for the interrelation of thermal anomalies with the electronic and spin-state transitions.

2 Experimental

Samples of $YCoO_3$, $DyCoO_3$, $GdCoO_3$, $SmCoO_3$, $NdCoO_3$, $PrCoO_3$ and $LaCoO_3$ were prepared by a solid state reaction from stoichiometric amounts of $Co(NO_3) \cdot 6H_2O$ and respective oxides Y_2O_3, Dy_2O_3, Gd_2O_3, Sm_2O_3, Nd_2O_3, Pr_6O_{11} and La_2O_3. The mixtures were first heated to 600 °C to remove nitrate. The resulting powder was pressed in the form of pellets and sintered at 900 °C (Y), 1000 °C (Dy, Gd, Sm, Nd and Pr) or 1200 °C (La) for 100 hours under oxygen flow.

X-ray diffraction confirmed single-phase character of the samples, except for $YCoO_3$, where about 2% of Y_2O_3 was detected in agreement with previous observations [12].

The temperature dependent structural characterization over the range 100–1000 K was performed using the X-ray powder diffractometer Bruker D8 (CuKα, energy dispersive SOL-X detector) equipped with a MRI TC-wide range temperature chamber. The measurements were performed under ambient atmosphere. Two scans were measured for each temperature, and the measured intensities compared in order to check whether the sample had not changed during the measurement of one temperature. The X-ray diffraction patterns were evaluated by Rietveld profile analysis using the FULLPROF program (version Mar98-LLB JRC).

Measurements of the electrical resistivity and thermoelectric power over the range 290–1000 K were done in a small tubular furnace with precisely controlled temperature. The standard K-type thermocouples (chromel – alumel) were used for monitoring of the sweeping temperature gradient ±5 K imposed across the sample by means of an additional heater. The voltage drop associated with thermal gradient was measured using chromel wires of the K-type thermocouple and chromel thermoelectric power was subtracted (based on Omega standard tables). The four-point steady state method for the electrical resistivity was applied.

The magnetic susceptibility of the $LaCoO_3$ and $YCoO_3$ compounds was measured on a SQUID magnetometer up to 400 K using a DC field 100 Oe and subsequently using 10 kOe in order to saturate the effect of small ferromagnetic impurities in the essentially diamagnetic phases (see also [13]). The high temperature data up to 900 K were obtained using a compensated pendulum system MANICS in a field of 19 kOe.

Thermogravimetric analysis (TGA) was performed in order to exclude the possible influence of changing oxygen stoichiometry. The TGA was measured using a 2960 SDT of TA Instruments using typically 50 mg sample in Pt pans. Corrections were made for the empty sample holder response. TGA was measured in air, under the same condition as HT-XRD, in the temperature range 573–1073 K. The maximum measured change of oxygen stoichiometry was found to be less than 0.1 mol%, i.e. below $\gamma = 0.003$ according to formula $LnCoO_{3-\gamma}$.

3 Results and discussion

The lattice parameters at room temperature of the $Pbnm$ compounds are plotted in Figure 1 as a function of the respective Ln^{3+} ionic radii (9-fold coordination). The observed values agree with other literature data [14]. It is useful to recall the Goldschmidt tolerance factor, which is a fundamental parameter determining the kind of structural distortion in perovskites with general formula ABO_3. It is defined as

$$t = \frac{r_A + r_O}{\sqrt{2}(r_B + r_O)} \quad (1)$$

where r_A, r_B and r_O are ionic radii of the respective cations and oxygen. The relation $b > c/\sqrt{2} > a$ observed from $YCoO_3$ to $SmCoO_3$ ($t < 0.92$) is typical for structures of so-called O-type, where buckling of the octahedra network is the dominant source of the orthorhombic distortion. The buckling becomes smaller with increasing size of the rare-earth cation and this effect is manifested by the linearly increasing average Co-O-Co bond

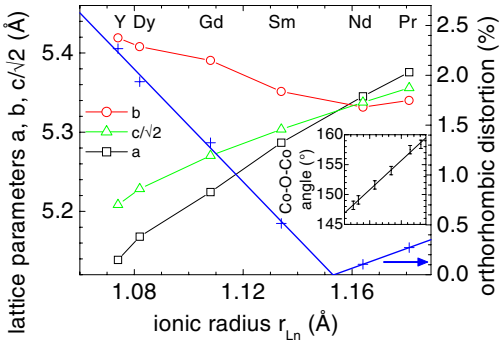

Fig. 1. Lattice parameters and orthorhombic distortion (Eq. (2)) vs. Ln ionic radius for $LnCoO_3$ (Ln = Y, Dy, Gd, Sm, Nd and Pr) at room temperature. All structures were refined within the *Pbnm* space group. The inset shows the average Co-O-Co bond angle. The scale of the x-axis of the inset is omitted and is identical with that of the main figure.

angle, see the inset of Figure 1. For $NdCoO_3$ and $PrCoO_3$ ($r_{Ln} > 1.15$ Å, $t > 0.92$) a small local distortion of the CoO_6 octahedra, namely deviation of the O-Co-O angle from 90°(common for orthoperovskites), starts to prevail over the buckling. As a consequence the relation of lattice parameters changes to $a > c/\sqrt{2} > b$.

Also displayed in Figure 1 is an orthorhombic distortion, which is defined as a standard deviation divided by an average of the lattice parameters

$$dist_{orth} = \frac{\sqrt{\sum (a_i - \overline{a})^2}}{\overline{a}} \qquad (2)$$

where $a_i = a$, b and $c/\sqrt{2}$ and $\overline{a}$ is the average of a_i. The orthorhombic distortion decreases linearly in the $b > c/\sqrt{2} > a$ region down to $r_{Ln} = 1.15$ Å, where the lattice parameters cross. In the $a > c/\sqrt{2} > b$ region it linearly increases, however with ≈ 3× smaller slope in absolute value.

No change of the crystal symmetry of the orthorhombic compounds was observed over the experimental temperature range, thus all the diffraction patterns were refined within the same *Pbnm* space group. The temperature evolution of lattice parameters of the *Pbnm* compounds is displayed in Figures 2 and 3. Since the first anomaly in thermal expansion of the rhombohedral $LaCoO_3$ is outside our experimental range, for this compound we used neutron diffraction data from [5].

For $YCoO_3$, $DyCoO_3$, $GdCoO_3$ and $SmCoO_3$ the relation $b > c/\sqrt{2} > a$ holds for all temperatures. Anomalous thermal expansion is manifested by a rapid S-shaped increase of the b lattice parameter, in agreement with previous reports [10,11]. This anomaly gives rise to a pronounced minimum in the temperature dependence of the orthorhombic distortion. Its position shifts to lower temperatures with increasing rare-earth ionic radius r_{Ln} from ≈600 K for $YCoO_3$ to ≈400 K for $SmCoO_3$. The temperature evolution of lattice parameters below this minimum reflects a higher thermal expansion of ionic Ln-O bonds compared to more covalent Co-O bonds. Consequently, the tolerance factor t increases with temperature and the orthorhombic distortion decreases with increasing temperature, resembling the room temperature dependence with increasing Ln ionic radius in Figure 1. On the other hand, the increase of orthorhombic distortion at high temperatures can be related to a gradual increase of Co-O bond lengths due to the spin-state transition of Co^{3+} ions,

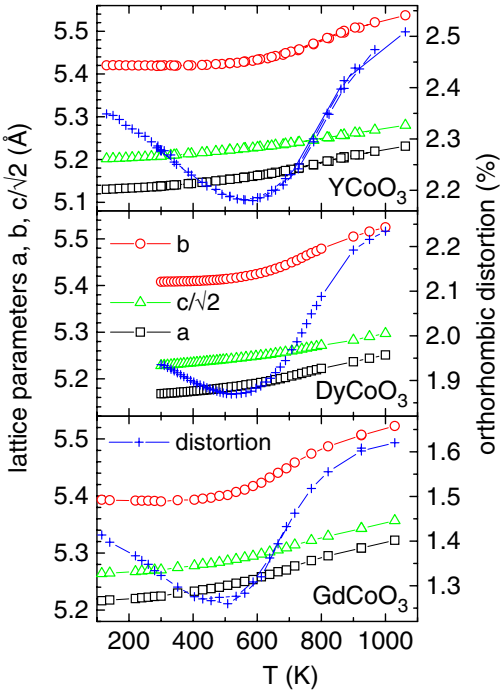

Fig. 2. Lattice parameters and orthorhombic distortion (Eq. (2)) vs. temperature for $YCoO_3$, $DyCoO_3$ and $GdCoO_3$.

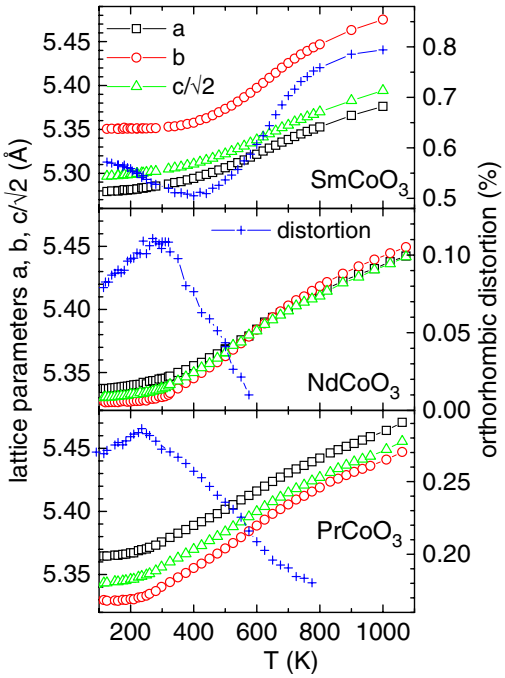

Fig. 3. Lattice parameters and orthorhombic distortion (Eq. (2)) vs. temperature for $SmCoO_3$, $PrCoO_3$ and $NdCoO_3$.

which is responsible for an anomalous decrease of t with temperature and has thus a similar effect as the decrease of r_{Ln} in Figure 1.

The behavior of orthorhombic distortions for $PrCoO_3$ and $NdCoO_3$ is apparently more complex. With increasing temperature they first increase going through a maximum at 230 K and 280 K, respectively, and then decrease. However, this is again in agreement with the dependence of the room temperature lattice parameters on r_{Ln}, as these phases belong to the region with $a > c/\sqrt{2} > b$, i.e. where orthorhombic distortion is increasing with r_{Ln}. In the case of $NdCoO_3$ lattice parameters cross around ≈600 K and above this temperature the relation changes to $b > c/\sqrt{2} > a$, which is typical for $LnCoO_3$ with smaller Ln.

The data on linear thermal expansions for $LnCoO_3$ (Ln = Y, Dy, Gd, Sm, Nd, Pr), completed with $LaCoO_3$ taken from [5], are displayed in Figure 4. Thermal expansion coefficients were calculated as an average over the main crystal directions using the formula

$$\alpha(T) = \frac{1}{l_o}\frac{l_2 - l_1}{T_2 - T_1}\ (\mathrm{K}^{-1}) \qquad (3)$$

where $l = (V/Z)^{1/3}$, V/Z is the cell volume per formula unit, l_o is the value at room temperature, l_2 and l_1 are values at two close temperatures T_2 and T_1, and $T = (T_1 + T_2)/2$.

Three essential features could be detected in the thermal expansions of $LnCoO_3$: (1) a linear increase of the expansion coefficient α, common within experimental error for all orthorhombic $LnCoO_3$, that starts from 100 K and spreads to about 500 K for Ln = Y and Dy. (2) A steep enhancement of α due to rapid increase of population of Co^{3+} IS or HS states, that rises from the linear section successively at higher temperatures as the Ln radius decreases. In the case of $LaCoO_3$ this steep enhancement occurs as low as 35 K (inflection point), so the linear part is missing. Corresponding inflection point temperatures of $PrCoO_3$ and $NdCoO_3$ are 230 K and 300 K, respectively. The steep enhancement of the expansion coefficient reaches a maximum clearly visible for $LaCoO_3$ and $PrCoO_3$, but only present as a shoulder for $NdCoO_3$ and becoming undetectable for still smaller Ln. (3) A broad maximum that shifts with decreasing Ln radius from ≈535 K for $LaCoO_3$ to ≈800 K for $YCoO_3$. Its height increases from 24×10^{-6} K^{-1} for $LaCoO_3$ to 42×10^{-6} K^{-1} for $GdCoO_3$ and then decreases for $DyCoO_3$ and $YCoO_3$.

The broad maximum of thermal expansion at high temperatures can be associated with the I-M transition [4]. This correspondence is also supported by comparison with an apparent activation energy E_A of the electric conduction, shown in the insets of Figure 4. The same trend in the peak position is observed, only the temperature of the activation energy maximum is 30–50 K lower than that of the thermal expansion. This suggests, together with the non-hysteretic character of the transition, that the conducting high-temperature state does not appear suddenly but is preceded by a phase separated mixture where the volume fraction of metallic regions grows gradually to beyond percolation. In the case of resistivity, the attainment of percolation is critical, whereas the thermal expansion reflects the bulk.

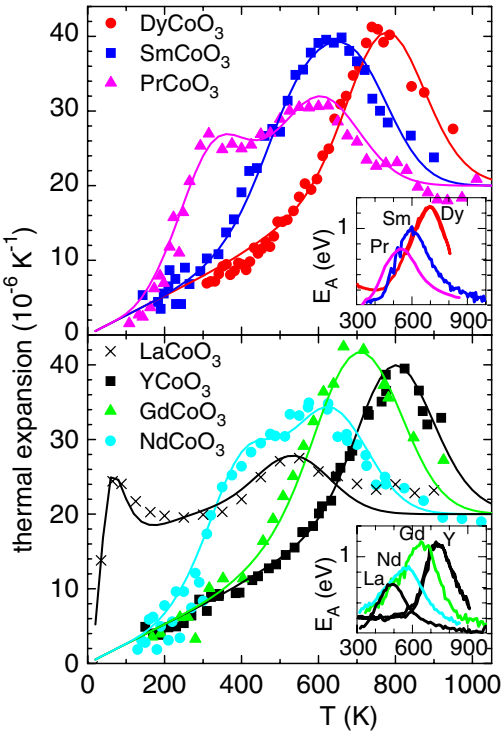

Fig. 4. Linear thermal expansion α (Eq. (3)) for $LnCoO_3$ and $LaCoO_3$ [5]. The solid lines are calculated fits of α. The inset shows apparent activation energy $E_A = d\ln\rho/d(T^{-1})$ calculated from resistivity ρ.

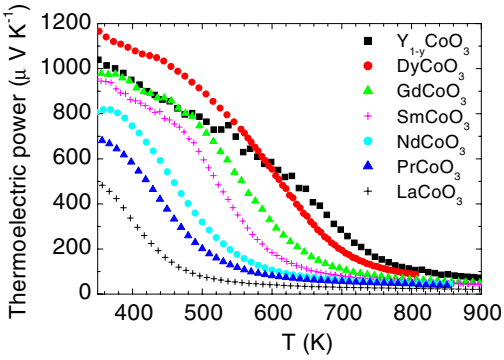

Fig. 5. High temperature thermoelectric power of $LnCoO_3$.

The phase separated onset of the conducting state in $LnCoO_3$ is further evidenced by a gradual change of thermoelectric power shown in Figure 5. The data confirm that the temperature of the I-M transition is increasing with decreasing rare-earth ionic radii. The deviation of $YCoO_3$ from the trend in absolute value of thermoelectric power is probably linked with the Y deficiency ($Y_{1-y}CoO_{3-\delta}$) mentioned above in the experimental section.

Magnetic susceptibility of $YCoO_3$ and $LaCoO_3$ is displayed in Figure 6. Raw susceptibility data contain the main temperature dependent contribution from the excited Co^{3+} states (IS or HS), the paramagnetic Van Vleck

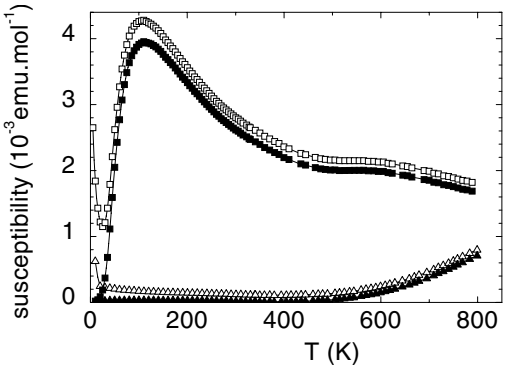

Fig. 6. Magnetic susceptibility of $YCoO_3$ (△) and $LaCoO_3$ (□). Raw data are displayed in open symbols, corrected data in full symbols.

susceptibility associated with the field-induced admixture of high-lying levels to the non-magnetic LS Co^{3+} ground state, the diamagnetic contribution of Co, O and Y or La core states and, finally, the contribution from paramagnetic impurities which is responsible for the hyperbolic increase of observed susceptibility (Curie-like term) at the lowest temperatures.

The raw data on $YCoO_3$ suggest that the sum of positive Van Vleck and negative diamagnetic terms is about 10^{-4} emu/mol, which gives $\chi_V \sim 2\times10^{-4}$ emu/mol in agreement with the theoretical prediction of Griffith and Orgel [15] and measurement of the NMR shift in spinel Co_3O_4 with LS Co^{3+} in octahedral sites by Kamimura [16]. After the subtraction these temperature independent terms and the above-mentioned impurity term, the corrected susceptibility is directly related to the number of excited Co^{3+} states $p(T)$ by the expression

$$\chi(T) = \frac{N_A\mu_B^2}{3k_B}\frac{g^2}{T}S(S+1)p(T) \qquad (4)$$

supposing, of course, a negligible interaction between excited species. Here, N_A is the Avogadro number, μ_B the Bohr magneton, k_B the Boltzmann constant, g is the Landé factor and S the spin number.

The fit we made to susceptibility data supposed a statistic ensemble of independent Co^{3+} ions with a non-magnetic (LS) ground state and a magnetic excited state. The population of excited states is then expressed by

$$p(T) = \frac{\nu(2S+1)e^{-E/T}}{1+\nu(2S+1)e^{-E/T}} \qquad (5)$$

where E is the energy difference between the ground and excited states in units of T, $2S+1$ and ν are the spin and orbital degeneracies of the excited state (the ground state is the spin and orbital singlet). We used $g = 2$ and $S = 1$, i.e. we supposed excited states of the IS character as in the paper of Zobel et al. [7]. Unlike this paper we allowed for a change of E with increasing temperature. In the calculation we used $\nu = 1$, which presumes that orbital degeneracy is lifted due to local distortions, either static or dynamic. This assumption is necessary for a

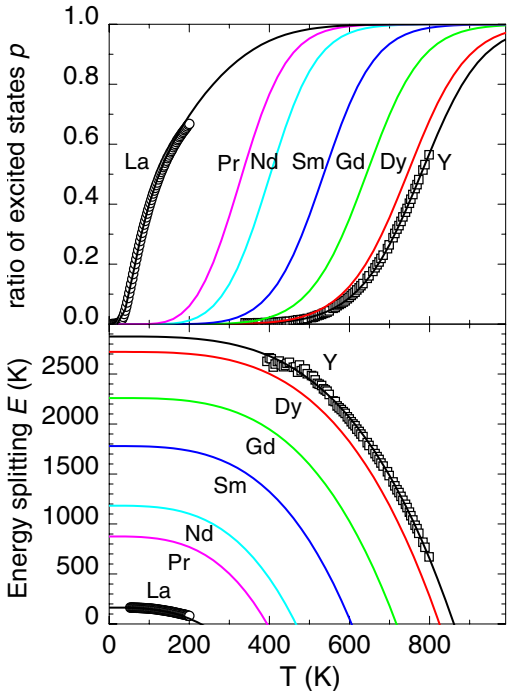

Fig. 7. Ratio of excited states p and energy splitting between ground and excited spin states E calculated from magnetic susceptibility for $YCoO_3$ and $LaCoO_3$ and interpolated for the other $LnCoO_3$.

consistent interpretation of the magnetic and thermal expansion $LaCoO_3$ data within the LS-IS scenario. For the magnetic transition in $YCoO_3$, which is at much higher temperature, the orbital degeneracy might be active, but has little effect for our analysis, except for some renormalization of the $E(T)$ values. Using the calculated $p(T)$ we derived the energy splitting of the ground and excited state as

$$E(T) = T\ln\left[\nu(2S+1)\frac{1-p(T)}{p(T)}\right]. \qquad (6)$$

The calculated $p(T)$ and $E(T)$ for $YCoO_3$ and $LaCoO_3$ are displayed in Figure 7. In both cases, $E(T)$ is a decreasing function, which can be related to a combined effect of normal and anomalous lattice expansion, and vanishes at some temperature T_o, corresponding to the LS-IS crossover (see also the electronic structure calculations in [17]). At T_o the actual IS/LS ratio is equal to $\nu(2S+1) = 3$. The energy $E(T)$ was arbitrarily fitted by a power function

$$E(T) = E_o\left[1-\left(\frac{T}{T_o}\right)^n\right] \qquad (7)$$

where E_o is the energy splitting at $T = 0$ K, T_o is the temperature where $E(T_o) = 0$ and n is a fitting parameter that describes the curvature. The dependencies of $E(T)$ on temperature for the other $LnCoO_3$ systems were estimated simply by a linear interpolation of E_o, T_o and n based on the ionic radii of Ln. The parameters, which are

Table 1. Ionic radii r_{Ln} for 9-fold coordination and the fit parameters of the analysis of magnetic and structural data of $LnCoO_3$: Energy splitting E_o of the ground and excited state at $T = 0$ K, temperature of LS-IS crossover T_o and power coefficient n, see equation (7). The temperature positions of maxima T_{mag} and T_{IM} of the α_{mag} and α_{IM} contributions, respectively.

	r_{Ln} (Å)	E_o (K)	T_o (K)	n	T_{mag} (K)	T_{IM} (K)
$YCoO_3$	1.075	2875	860	3.51	780	800
$DyCoO_3$	1.083	2721	825	3.48	740	785
$GdCoO_3$	1.107	2260	717	3.39	619	740
$SmCoO_3$	1.132	1779	605	3.29	493	693
$NdCoO_3$	1.163	1183	466	3.17	337	635
$PrCoO_3$	1.179	875	395	3.11	256	605
$LaCoO_3$	1.216	164	230	2.97	70	535

summarized in Table 1, were subsequently used for calculation of $p(T)$ curves using equation (5).

With the knowledge of $p(T)$ in hand, the model for the thermal expansion of $LnCoO_3$ can be divided into a three contributions

$$\alpha(T) = \alpha_{latt} + \alpha_{mag} + \alpha_{IM}. \tag{8}$$

(1) Lattice term α_{latt} is a weighted sum by $p(T)$ of normal thermal expansions of $LnCoO_3$ in LS state (α_{LS}) and in excited spin state (α_{IS})

$$\alpha_{latt}(T) = \alpha_{LS}(T)[1 - p(T)] + \alpha_{IS}(T)p(T). \tag{9}$$

(2) The anomalous contribution α_{mag} is related to the temperature change of the amount of excited states, given by a temperature derivative of equation (5)

$$\frac{\partial p}{\partial T} = \frac{\nu(2S+1)e^{-E/T}}{(1+\nu(2S+1)e^{-E/T})^2}\left(\frac{E}{T^2} - \frac{1}{T}\frac{\partial E}{\partial T}\right) \tag{10}$$

and can be expressed as

$$\alpha_{mag}(T) = \frac{\partial p}{\partial T}\, d_{mag} \tag{11}$$

where $d_{mag} = (l_{IS} - l_{LS})/l_o$.

(3) The contribution α_{IM} refers to the anomalous expansion associated with the I-M transition. For our analysis the α_{IM} term was modelled rather arbitrarily by a Gaussian profile

$$\alpha_{IM}(T) = \frac{d_{IM}}{h_{IM}}\sqrt{\frac{4\ln 2}{\pi}}\, e^{-4\ln 2\left(\frac{T-T_{IM}}{h_{IM}}\right)^2} \tag{12}$$

where d_{IM} is the total area and h_{IM} is the width of the Gaussian profile at the half maximum.

From the character of thermal expansion shown for the Sm, Gd and Y compounds in Figure 4 we infer that the lattice contribution α_{LS} is linearly increasing at least up to ≈400 K and above ≈600 K it levels at about $\alpha_{LS} = 14 \times 10^{-6}$. For α_{IS} we expect a similar trend on the basis of data used for $La_{0.82}Sr_{0.18}CoO_3$ in [7], but with larger slope and larger saturation, $\alpha_{IS} > \alpha_{LS}$. Since the excited magnetic state dominates for all $LnCoO_3$ systems at elevated temperatures, our data in Figure 4 actually show that the expansion coefficient saturates at a value $\alpha_{IS} = 20 \times 10^{-6}$. A somewhat larger experimental value for $LaCoO_3$ is derived from data of reference [5] but this is most likely due to a partial reduction $Co^{3+} \rightarrow Co^{2+}$ at high temperatures, caused by the neutron diffraction measurement in vacuum.

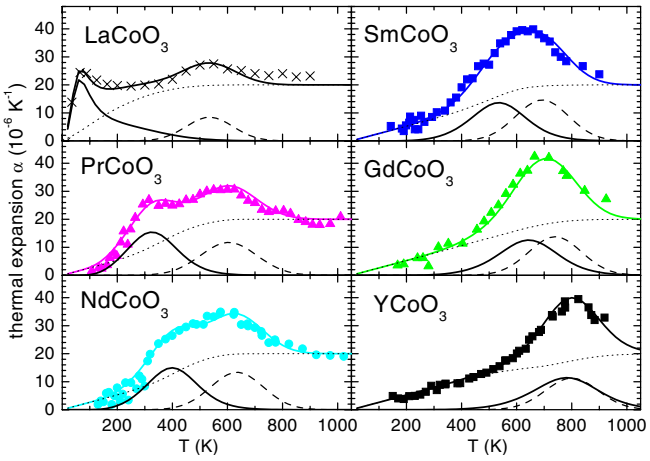

Fig. 8. The fits of thermal expansion and the three contributions α_{latt} (···), α_{mag} (—) and α_{IM} (- - -).

The fits of thermal expansion including all three contributions α_{latt}, α_{mag} and α_{IM} are displayed in Figure 8. The contributions associated with the diamagnetic-paramagnetic and I-M transitions are characterized with the temperature position of the maxima, T_{mag} and T_{IM}. They are found to increase linearly with decreasing Ln radius (see Tab. 1). The shape of α_{mag} is fitted with parameters E_o, T_o and n as shown in the expression for $E(T)$ above, while the presumed Gaussian profile of α_{IM} is well fitted with practically constant width for all $LnCoO_3$ $h_{IM} \sim 225$ K. The integral expansion is quantified by parameters $d_{mag} = 0.35\%$ and $d_{IM} \sim 0.32\%$, showing that the linear change of the perovskite cell upon the first and second transition is of similar extent. The corresponding volume change is roughly 1% in both cases. Considering that lattice expansion is mostly due to increase of the bond valence length Co-O (see structural data for $LaCoO_3$ [5] in Fig. 9), we can estimate that the Co^{3+} ionic radius is changed from 0.545 Å for LS state to 0.552 Å and 0.558 Å after the diamagnetic-paramagnetic and I-M transitions, respectively.

It should be noted that our value d_{mag} is smaller than $d = 0.66\%$ reported previously for $LaCoO_3$ by Zobel et al. in [7] on the basis of their dilatometric measurements. This difference has two origins. First, the present expansion data for $LaCoO_3$ deduced from neutron diffraction [5] are about 1.5× lower than the dilatometric data. The second difference is that they supposed constant energy splitting E whereas we allow decrease of E with temperature. As to energy splitting E_o at absolute zero between the LS ground state and excited magnetic state, our values in

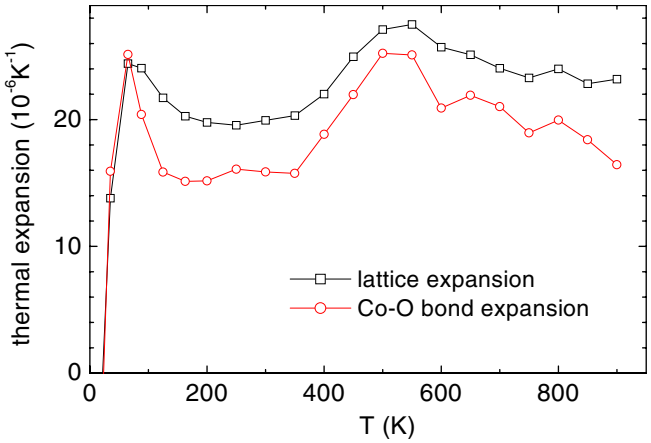

Fig. 9. Comparison of the lattice (□) and Co-O bond distance (○) thermal expansions in $LaCoO_3$.

Table 1 are in good agreement with previously reported data. The energy splitting E_o for $LaCoO_3$ was determined to be 180 K in [2], 185 K in [7] and 190 K in [18], in all cases with $S = 1$ and $\nu = 1$. These values are in quite good agreement with our value of 164 K. The energy splitting for $EuCoO_3$ was calculated assuming orbital degeneracy $\nu = 3$ in [18]. As we mentioned above, using $\nu = 3$ for analysis of our susceptibility of $YCoO_3$ only renormalizes the energy, namely E_o increases to 3220 K, but does not alter the evolution of $E(T)$. With this value the interpolation with respect to Eu ionic radius gives $E_o = 2250$ K for $EuCoO_3$, close to the value of 1900 K obtained in [18]. An energy splitting of 1095 K calculated for $PrCoO_3$ in [2] is also quite close to our value of 875 K. However $E_o = 2750$ K for $NdCoO_3$ determined in [2] is much higher than the values obtained by our analysis, and also does not agree with [18], since the energy splitting of $NdCoO_3$ is not expected to be higher than that of $EuCoO_3$.

4 Conclusion

An X-ray diffraction study was performed on a series of $LnCoO_3$ perovskites (Ln = Y, Dy, Gd, Sm, Nd, Pr and La) over a broad range of temperatures up to 1000 K. Structural effects associated with the spin-state transitions of Co^{3+} ions, in particular the anomalous thermal expansion, were analyzed in combination with electric transport measurements and, for Ln = Y and La, with the magnetic susceptibility data. As a result, the temperature dependence of linear expansion coefficients of $LnCoO_3$ were fitted using a small number of parameters which are either constant — d_{mag} and d_{IM} — or depend linearly on the Ln ionic radius — E_o, T_o and T_{IM}. The observed expansion is a sum of three contributions:

1. A weighted sum of the lattice expansions of cobaltite in the diamagnetic LS state and in the paramagnetic IS or HS state.
2. The anomalous contribution due to increasing population and subsequent stabilization of the excited IS or HS states at the course of the diamagnetic-paramagnetic transition.
3. The anomalous contribution due to the I-M transition, associated with a further change of the paramagnetic state.

The analysis shows that the volume change during two successive magnetic and electronic transitions is independent of the kind of Ln cation and, interestingly, it is of similar amplitude in both cases, namely 1%. In a linear dimension, this volume increase corresponds to a change of the Co^{3+} ionic radius from 0.545 Å for LS state to 0.552 Å and 0.558 Å after the diamagnetic-paramagnetic and I-M transitions, respectively. This change is too small to be compared with the radius of Co^{3+} ions in a HS state ($r_{HS} = 0.61$ Å). The expansion data are thus in favor of the IS ($r_{IS} = 0.56$ Å) nature of magnetic Co^{3+} species in $LnCoO_3$.

Within such an LS-IS scenario of the first transition, the present model calculations provide the values of the LS-IS gap and their evolution with temperature, and allow estimation of the temperature rate of IS population during the magnetic transition in $LnCoO_3$ compounds where investigation of the Co^{3+} magnetism is hindered due to a much larger rare-earth contribution.

The nature of the second transition is still under question. Although we denote it as insulator-metal, it is associated with a kind of magnetic transition, which is clearly evident on the susceptibility behavior of $LaCoO_3$. The insulator-metal transition itself should not be accompanied by a positive contribution to thermal expansion. We suppose, therefore, that, similarly to the first transition, the I-M transition for all $LnCoO_3$ originates in thermal excitations to another paramagnetic state separated by energy splitting which vanishes with temperature.

The work was supported in part by the European Community's Human Potential Programme under contract HPRN-CT-2002-00293, SCOOTMO. We acknowledge support of AS CR within the Project No. AV0Z10100521.

References

1. J. Hejtmánek, Z. Jirák, K. Knížek, M. Maryško, M. Veverka, H. Fujishiro, J. Magn. Magn. Mat. **272-276**, E283 (2004)
2. J.-Q. Yan, J.-S. Zhou, J.B. Goodenough, Phys. Rev. B **69**, 134409 (2004)
3. L. Sudheendra, M.M. Seikh, A.R. Raju, C. Narayana, Chem. Phys. Lett. **340**, 275 (2001)
4. S. Yamaguchi, Y. Okimoto, Y. Tokura, Phys. Rev. B **54**, R11022 (1996)
5. P.G. Radaelli S.-W. Cheong, Phys. Rev. B **66**, 094408 (2002)
6. G. Maris, Y. Ren, V. Volotchaev, C. Zobel, T. Lorenz, T.T.M. Palstra, Phys. Rev. B **67**, 224423 (2003)
7. C. Zobel, M. Kriener, D. Bruns, J. Baier, M. Grüninger, T. Lorenz, P. Reutler, A. Revcolevschi, Phys. Rev. B **66**, R020402 (2002)

8. K. Asai, O. Yokokura, N. Nishimori, H. Chou, J.M. Tranquada, G. Shirane, S. Higuchi, Y. Okajima, K. Kohn, Phys. Rev. B **50**, 3025 (1994)
9. K. Asai, A. Yoneda, O. Yokokura, J.M. Tranquada, G. Shirane, K. Kohn, J. Phys. Soc. Jpn. **67**, 290 (1998)
10. X. Liu, C. Prewitt, J. Phys. Chem. Solids **52**, 441 (1991)
11. G. Demazeau, M. Pouchard, P. Hagenmuller, J. Solid State Chem. **9**, 202 (1974)
12. A. Mehta, R. Berliner, R. Smith, J. Solid State Chem. **130**, 192 (1997)
13. J.-Q. Yan, J.-S. Zhou, J.B. Goodenough, Phys. Rev. B **70**, 014402 (2004)
14. *Inorganic Crystal Structure Database. National Institute of Standards and Technology (NIST) and Fachinformationszentrum Karlsruhe (FIZ)* (version 2004)
15. J.S. Griffith, L.E. Orgel, Trans. Faraday Soc. **53**, 601 (1957)
16. H. Kamimura, J. Phys. Soc. Jpn. **21**, 484 (1966)
17. M.A. Korotin, S.Y. Ezhov, I.V. Solovyev, V.I. Anisimov, D.I. Khomskii, G.A. Sawatzky, Phys. Rev. B **54**, 5309 (1996)
18. J. Baier, S. Jodlauk, M. Kriener, A. Reichl, C. Zobel, H. Kierspel, A. Freimuth, T. Lorenz, Phys. Rev. B **71**, 014443 (2005)